Topochemical Correlation between Carbohydrates and Lignin in *Eucommia ulmoides* Cell Wall from Tissue to Cell Level

Kexia Jin, Heshuai Cui, Xinge Liu,* and Jianfeng Ma *

The efficient conversion of biomass into biofuels is closely associated with the topochemistry of the cell wall. In this study, the topochemical correlation between carbohydrates and lignin in the *Eucommia ulmoides* cell wall was investigated *in situ* by confocal Raman microscopy. The carbohydrates and lignin were mainly collocated in the secondary wall of the fiber, ray parenchyma, and vessel in *E. ulmoides*. High carbohydrates were associated with low lignin or *vice versa*, indicating that a high concentration of carbohydrates leads to a drop in the degree of lignification. Furthermore, the band intensity ratio of S- and G-lignin to carbohydrates (I_{1333}/I_{2889} and I_{1274}/I_{2889}) in morphologically distinct regions of fiber was calculated. In accordance with the wet chemical analysis, a higher ratio of lignin to carbohydrates was observed within the middle layer of the 3-year-old *E. ulmoides* fiber secondary wall. The results potentially extend the current understanding of the carbohydrate and lignin topochemistry in woody biomass and may facilitate an efficient wood bioconversion process in future biorefineries.

Key words: Raman imaging; Topochemical correlation; Carbohydrates; Lignin

*Contact information: Key Lab of Bamboo and Rattan Science and Technology, International Centre for Bamboo and Rattan, Beijing 100102, China; *Corresponding author: mjfxl31@126.com; liuxe@icbr.ac.cn*

INTRODUCTION

The cell wall of lignocellulosic biomass is primarily composed of cellulose, lignin, and hemicelluloses. Carbohydrates (cellulose and hemicelluloses) can be hydrolyzed into fermentable sugars and further processed into bioethanol and other biofuels (Zeng *et al.* 2014). However, carbohydrate bioconversion is hindered by the complex structure and distribution of heterogeneous components within cell walls. Lignin fills the voids between carbohydrates in the plant cell wall, which creates highly natural biomass recalcitrance that reduces their accessibility to carbohydrate-modifying enzymes. Lignin content is the key factor that is negatively correlated with enzyme digestibility and sugar release (Song *et al.* 2015; Yu *et al.* 2015; Raut *et al.* 2016). With less than 20% lignin content in *Populus*, the sugar yield increases significantly for enzymatic hydrolysis even without pretreatment (Studer *et al.* 2011). Thus, research on the correlation between carbohydrates and lignin is of great importance for biofuel production.

Most traditional chemical analyses of plant cell walls are destructive because they require disintegration of the plant tissue or the tissue sectioning by embedding the samples (Yuan *et al.* 2011; Moniz *et al.* 2015; Xu *et al.* 2015). In addition, sample isolation difficulties arise when small cell wall areas or single layers are of interest because they have to be carefully excised. Advances in confocal Raman microscopy and imaging have tackled this problem in a noninvasive way to provide chemical and structural information *in situ*

with a high spatial resolution (< 0.5 μm) (Agarwal *et al.* 2011; Richter *et al.* 2011; Prats *et al.* 2016). Both lignin and carbohydrates can be mapped simultaneously by selecting the Raman bands that are specific to these cell wall components. Although a number of early investigations established the distribution of carbohydrates and lignin by using confocal Raman microscopy and imaging (Agarwal 2006; Kim *et al.* 2012; Andersson *et al.* 2015b), little information is available on the correlation between the concentration of these two polymers in different tissues and morphologically distinct cell wall layers.

In this study, the correlation between carbohydrates and lignin was examined for the first time on the *E. ulmoides* cell wall. This study provided the theoretical basis and experimental evidence for designing efficient process of converting lignocellulosic biomass.

EXPERIMENTAL

Materials

Eucommia ulmoides was obtained from Yangling, Shanxi, China, and cut down at breast height (1.3 meters) in May 2015. The bark and leaves were removed, and only the stalks were used. Small sample blocks (1.5 cm × 1.0 cm × 2.0 cm) of 3-year-old and 1-year-old *E. ulmoides* were cut from the tenth column cell near the pith (Fig. 1). Approximately 5 μm-thick cross-sections were cut from the sample blocks using a sliding microtome (Leica RM2010R, Wetzlar, Germany). For chemical imaging, the samples were placed on a glass slide with a drop of D_2O, covered by a coverslip (0.17 mm thickness), and sealed with nail polish to prevent evaporation during measurement. Immersion in D_2O can effectively limit laser-induced fluorescence (Atalla and Agarwal 1986).

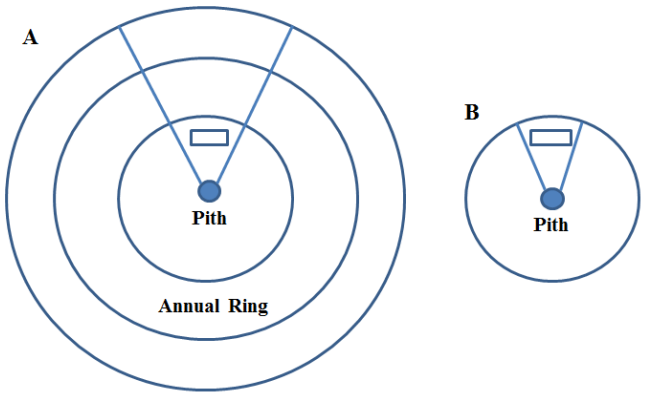

Fig. 1. The model of obtaining small sample blocks from 3-year-old (A) and 1-year-old (B) *E. ulmoides*

Methods

Compositional analysis

The compositions of the samples were determined as previously described (Sluiter *et al.* 2008). They were analyzed by high-performance anion exchange chromatography (HPAEC) (Dionex, ICS 3000, Sunnyvale, CA, USA) on a CarboPac PA 20 analytical column (4 mm × 250 mm) with pulsed-amperometric detection (PAD).

Morphological and anatomical characterization

To evaluate fiber morphology, the stems were manually cut into 2.5 mm × 2.5 mm × 30 mm strips. The samples were treated with acetic acid and 30% hydrogen peroxide (1:1, v/v) at 60 °C for 24 h for cell dissociation. After turning white in color, the samples were stirred vigorously in order to separate single cells. The macerated samples were thoroughly washed with distilled water, then stained with a Herzberg reagent and mounted onto microscope slides. The morphological features were measured using a Leica DM2500 light microscope (Wetzlar, Germany) at different magnifications. The anatomical observations were carried out on transverse sections. The sections were stained with Safranin O and mounted in glycerol on the glass slide, dehydrated in a graded ethanol (50%, 70%, 90%, 95%, and 100%), covered by a coverslip, and sealed with nail polish to avoid evaporation.

The proportion of tissue in different cell types was calculated on transverse sections by using the NIS-Elements imaging software (Nikon, Tokyo, Japan). Vessels were distinguished from fibers and axial parenchyma by defining 469 μm^2 as the smallest vessel lumen area, based on preliminary measurements. The short parenchyma cells of each cross section, and then the vessels, were "painted" on the computer screen by the computer operator. Their area relative to the whole section was then assessed by the program. The fiber proportion was obtained by subtracting proportional areas of vessel and parenchyma from unity (100%).

Topochemical distribution of cell wall components

The topochemistry of the *E. ulmoides* cell wall was investigated by confocal Raman microscopy. The Raman spectra were acquired with a LabRam Xplora confocal Raman microscope (Horiba Jobin Yvon, Paris, France). For high spatial resolution, the measurements were conducted with an Olympus high numerical aperture (NA) microscope objective (MPlan 100 ×, Oil, NA= 1.40; Olympus, Tokyo, Japan) and a linear-polarized 532 nm laser. For mapping, 0.5 μm steps were chosen, and every pixel corresponded to one scan. The spectrum from each location was obtained by averaging 2-second cycles. Different chemical images were generated by a cosmic ray removal filter, and default software sum filters (Labspec5, Horiba, Kyoto, Japan) were applied to integrate the defined regions in the wood spectra. The filter calculates the intensities within the chosen areas, and the background is subtracted by taking the baseline from the first to the second border. The overview chemical images separated cell wall layers and marked the defined distinct cell wall areas to calculate the average spectra from the areas of interest. Before a detailed analysis, the calculated average spectra were baseline corrected using the Savitsky-Golay algorithm (lines-method, 7 points). To determine the Raman peak intensity ratio, the resulting spectra were de-convoluted across the frequency ranges 1415 cm^{-1} to 1195 cm^{-1}. The de-convolution of the spectra by peak fitting was performed using a Gaussian-Lorentz model. The peak area of the Raman band was then determined.

RESULTS AND DISCUSSION

Anatomical and Morphological Features

Eucommia ulmoides is a diffuse-porous wood with distinct growth ring boundaries in the transverse section, as shown in Fig. 2A. Radial multiple pores are common; there are some solitary vessels, which are circular to angular in the transectional outline. Xylem rays have mainly two types, uniseriate and biseriate. As observed under a light microscope, it

has basic tissues containing libriform fibers for strength (Fig. 2B). In addition to the fiber, other cell types were evident, including short parenchyma and vessel.

According to the measurement of various cell areas in the 3-year-old samples, the proportion of different cell types both in early wood and late wood are shown in Table 1. In the 1-year-old and 3-year-old *E. ulmoides*, the fiber occupies major proportion of the tissues to support the hardwood.

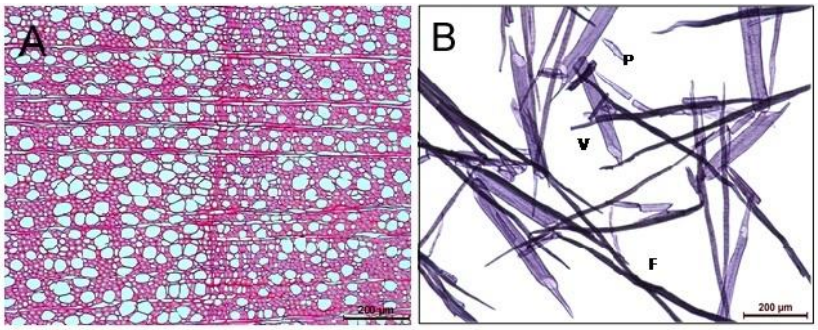

Fig. 2. Anatomy of *E. ulmoides* in a transverse section (A), and morphological features (B); V: vessel; F: fiber; and P: parenchyma

Table 1. The Proportion of Different Cell Types in Early Wood and Late Wood for 3-year-old and 1-year-old *E. ulmoides*

Proportion (%)	Early Wood		Late Wood	
	1-year-old	3-year-old	1-year-old	3-year-old
Fiber	56.3	58.2	66.1	68.1
Vessel	38.2	36.9	32.6	29.6
Short Parenchyma	5.5	4.9	1.3	2.3

Raman Spectra of *E. ulmoides* Cell Wall

The average spectra were calculated for the various cell types (fiber, vessel, axial parenchyma, and ray parenchyma) of *E. ulmoides* (Figs. 3A, B). A strong band was observed at 2889 cm^{-1}, which was assigned to the stretching of the C-H and C-H_2 groups. The peaks at 1097 cm^{-1} and 1122 cm^{-1} were attributed to the asymmetric and symmetric stretch of the C-O-C linkages, respectively. A band at 1377 cm^{-1} was attributed to the HCC, HCO, and HOC bending. All of these peaks are assigned to carbohydrates (Agarwal and Atalla 2010; Larsen and Barsberg 2010; Zhang *et al.* 2014). There was a dominant shoulder around 2936 cm^{-1} that was assigned to the C-H stretch of the methoxyl groups of the lignin. The peak at 1656 cm^{-1} represented stretching vibrations of the ring-conjugated C=C bonds in the coniferyl alcohol and sinapyl alcohol. A strong band was observed around 1598 cm^{-1} in all spectra, which was assigned to an aromatic ring stretch, and also gave rise to a band at 1193 cm^{-1} (a phenol mode). These peaks corresponded to lignin (Agarwal *et al.* 2011; Sun *et al.* 2012; Kanbayashi and Miyafuji 2015). Moreover, the shoulders at 1274 cm^{-1} and 1333 cm^{-1} were signature peaks for a guaiacyl ring mode (G-lignin) and an aliphatic O-H bend (S-lignin), respectively. Although cellulose and xylan might contribute to this area, the bands from the G- and S-lignin did not overlap with cellulose (1294 cm^{-1}) and xylan (main hemicelluloses in hardwood, 1267 cm^{-1}) when deconvoluting the Raman spectra ranging from 1415 cm^{-1} to 1195 cm^{-1} (Fig. 3C). Thus, it is appropriate to use these two peaks to investigate the G- and S-lignin.

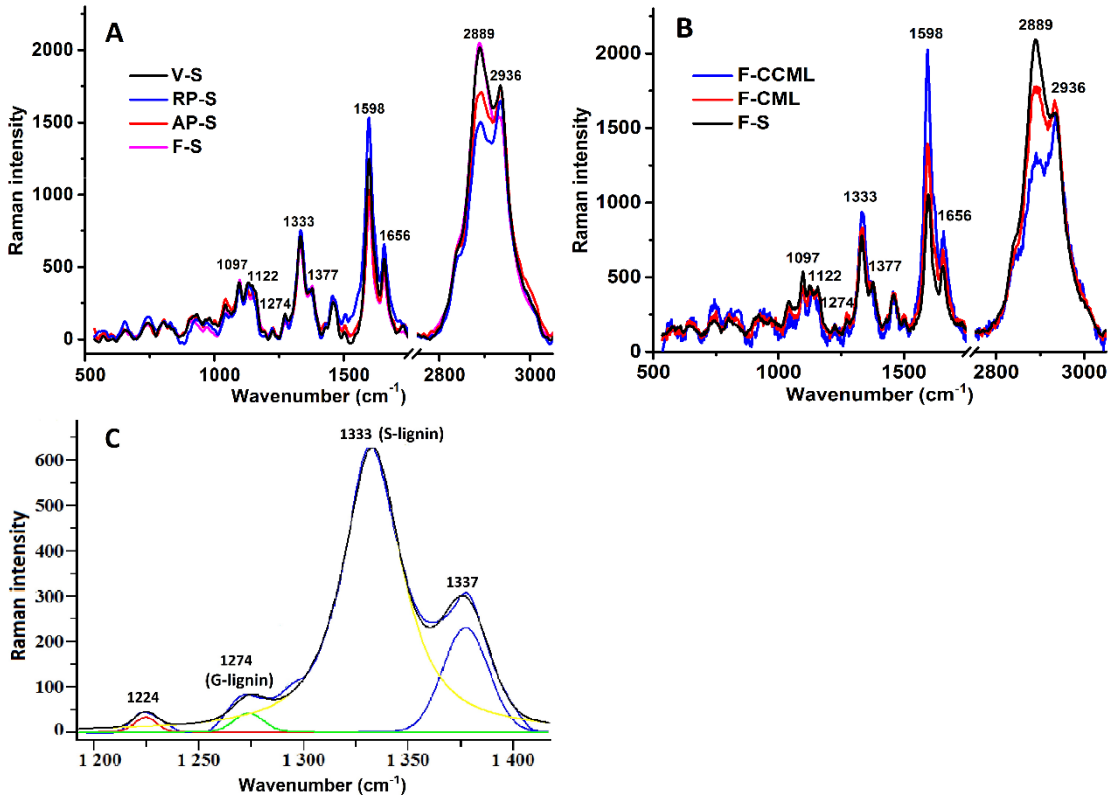

Fig. 3. Raman spectra of various cell types (A) and morphologically distinct regions of the fiber cell wall (B). Deconvolution Raman spectra ranging from 1195 cm^{-1} to 1415 cm^{-1} (C). F: fiber; V: vessel; AP: axial parenchyma; RP: ray parenchyma; S: the secondary wall; CCML: cell corner middle lamella; and CML: compound middle lamella

Topochemical Correlation between Carbohydrates and Lignin in *E. ulmoides* Cell Wall

For an overview of the measurement areas, the Raman images with all cell wall structures were calculated by integrating over the CH and CH_2 stretching vibrations (2920 cm^{-1} to 2768 cm^{-1}). The various cell types and morphologically distinct regions of the fiber cell wall were clearly visualized by Raman imaging (Fig. 4A). High intensity and thus high carbohydrate concentration were observed especially in the secondary wall of fiber and vessel, whereas the ray and axial parenchyma showed lower concentration. Within the sub-cellular level, the highest intensity was found in the fiber secondary wall (S-O: Outer-layer; S-M: Middle-layer; S-I: Inner-layer), followed by the compound middle lamella (CML), and the lowest in the cell corner middle lamella (CCML). A Raman image by calculating the band ranges from 1660 cm^{-1} to 1543 cm^{-1} also displayed the heterogeneity in lignin distribution (Fig. 4B), with a higher intensity in the CCML, CML, and S-I. The overlay image shown in Fig. 4C reveals the colocalization of carbohydrates and lignin. They were colocalized mainly in the secondary wall of fiber, ray parenchyma, and vessel, where carbohydrates are highly enriched and lignin deposition is lower. In contrast, where there is little or no colocalization in other cell regions (CCML, CML, and axial parenchyma) and the carbohydrate concentration is low, by comparison, lignification was obvious. The overlay image suggests that high carbohydrates were associated with low lignin or *vice versa*.

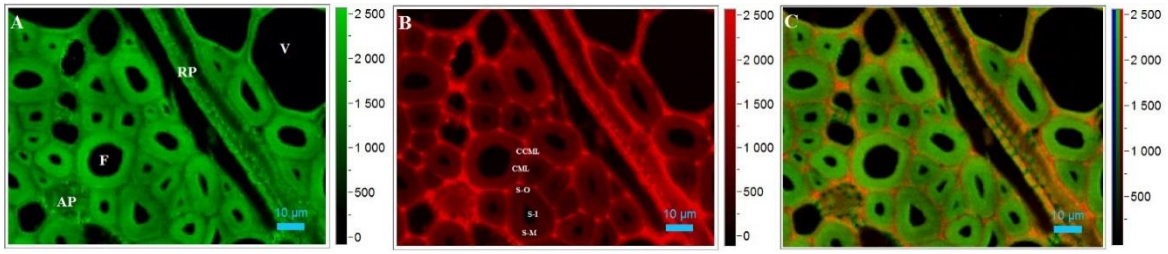

Fig. 4. Raman images of various cell types for *E. ulmoides* that were calculated by integrating from 2920 cm^{-1} to 2768 cm^{-1} (A, carbohydrates) and from 1660 cm^{-1} to 1543 cm^{-1} (B, lignin); (C) overlay images of lignin and carbohydrates colocalization. F: fiber; V: vessel; AP: axial parenchyma; RP: ray parenchyma; CCML: cell corner middle lamella; CML: compound middle lamella; S-O: outer-layer; S-M: middle-layer; and S-I: inner-layer

Donaldson and Knox (2012) compared the localization of cell wall polysaccharides in both normal and compression wood and found that polysaccharides were colocalized with lignin in the secondary cell wall. More highly lignified wall layers had less or no mannan, and less lignified layers had increased mannan, as shown by fluorescence microscopy combined with immunocytochemistry. Carbohydrates influence lignin polymerization (Yin *et al.* 2004; Jungnikl *et al.* 2008; Hu *et al.* 2016). In the middle lamella region, where carbohydrates have a low concentration, lignin deposition occurred by the addition of proto-lignin monomers to the spherical particles of lignin. However, lignification in the secondary wall, where the carbohydrate concentration is high, showed greatly elongated patches of lignin due to the greater rate of deposition along the microfibril axis. In the secondary wall where lignin deposition occurs, the cellulose matrix exerts a mechanical influence that limits the rate of lignin deposition in the direction perpendicular to the microfibril axis (Donaldson 1993). In addition, the orientation of cellulose may also impact lignin polymerization. High lignification was exhibited in the CCML and CML regions, where cellulose has little or no orientation. In contrast, there is slight lignification in the secondary wall of fiber where cellulose is highly oriented in a S-Z-S helical organization (Agarwal 2006). Hence, it is possible that a high concentration of carbohydrates results in decreased lignification.

Through wet chemistry techniques, the proportion of lignin (30.86%) and carbohydrates (63.2%) in 3-year-old *E. ulmoides* was calculated. In 1-year-old *E. ulmoides*, the corresponding values were 26.29% and 68.1%, respectively. Li and Lei (2016) also calculated the lignin and carbohydrates proportion of *E. ulmoides* at different age; the results showed a similar trend, indicating that younger trees had lower lignin content. However, the results averaged out the diversity of chemical information across all tissue types. Lignin and carbohydrates were heterogeneously distributed within the cell wall, which was confirmed by Raman imaging (Figs. 4A-4C). To further explore the concentration correlation between the lignin and carbohydrates at cellular and sub-cellular levels, the band intensity ratio of 1598 cm^{-1} (lignin), 1333 cm^{-1} (S-lignin), and 1274 cm^{-1} (G-lignin) to 2889 cm^{-1} (carbohydrates) in the Raman spectra were calculated (I_{1598}/I_{2889}, I_{1333}/I_{2889}, and I_{1274}/I_{2889}, respectively). Because the fiber takes up the major proportion of the tissues (Table 1), only the fiber was investigated thoroughly in this area. As shown in Figs. 5A and 5B, the ratios within the morphologically distinct cell wall layers of the *E. ulmoides* fiber varied remarkably. Semi-quantitative results indicated that the band intensity ratio (I_{1598}/I_{2889}) in the middle lamella (CCML and CML) of the 3-year-old *E. ulmoides* was lower than that of the 1-year-old *E. ulmoides*, suggesting a lower relative lignin concentration (Fig. 6A).

Although the S-O and S-I displayed a lower ratio in the 3-year-old *E. ulmoides*, the S-M containing the majority of the mass of wood had a higher ratio. Combining the results from the tissue proportion (Table 1) with the analysis of the lignin-to-carbohydrate ratio at a cellular level further supports the wet chemistry analysis.

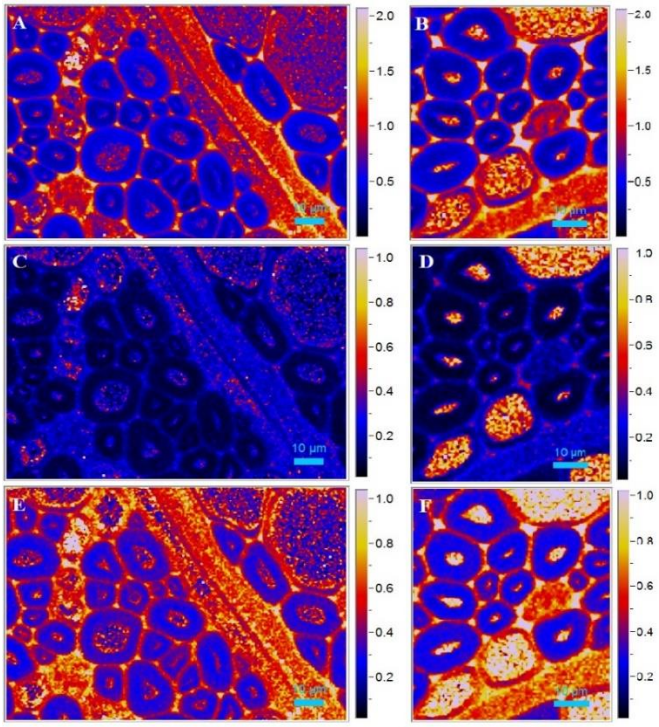

Fig. 5. The concentration ratio of lignin to carbohydrates (A, B: I_{1598}/I_{2889}; C, D: I_{1333}/I_{2889}; E, F: I_{1274}/I_{2889}) of various cell types and morphologically distinct regions of fiber cell wall in 3-year-old *E. ulmoides* (A, C, E) and 1-year-old *E. ulmoides* (B, D, F)

The S- and G-lignin-to-carbohydrate ratio for the *E. ulmoides* spectra was calculated as follows. First, the region between 1195 cm^{-1} and 1415 cm^{-1} was fitted to a set of four Gaussian distributions, which included peaks at 1274 cm^{-1} and 1333 cm^{-1} to represent the G- and S-lignin, respectively. The S- and G-lignin-to-carbohydrate ratios were calculated by using the area under the S-lignin, G-lignin, and carbohydrates. The Gaussians peaks are shown in Figs. 5C through 5F. The S- and G-lignin-to-carbohydrate molar ratios were calculated as 0.33 and 0.10, respectively, in the fiber S-M of the 3-year-old *E. ulmoides*. This was higher than that of the 1-year-old *E. ulmoides* in the corresponding areas (Figs. 6B and 6C). Interestingly, the S-O and S-I showed the opposite trend with the higher ratio in the 1-year-old *E. ulmoides*. Previous investigations indicated that the cell wall components deposited in a certain sequence (Marjamaa *et al.* 2003; Zeng *et al.* 2014). During wood cell wall formation, the incorporation of lignin within the polysaccharide cell wall framework is the final stage of differentiation in the secondary xylem cell wall. Lignin polymerization starts first in the CML and CCM, and subsequently spreads into the secondary wall. Within the secondary wall, a preferable deposition of non-condensed G- and S-lignin in the S1 and S3 layers at the initial stage of cell wall differentiation was visualized, accompanied by the incorporation of condensed G and S subunits with a rather weak labelling within the entire S2 layer (Ruel 2004). These findings can explain the higher ratio in the S-O and S-I of the 1-year-old *E. ulmoides* fiber wall.

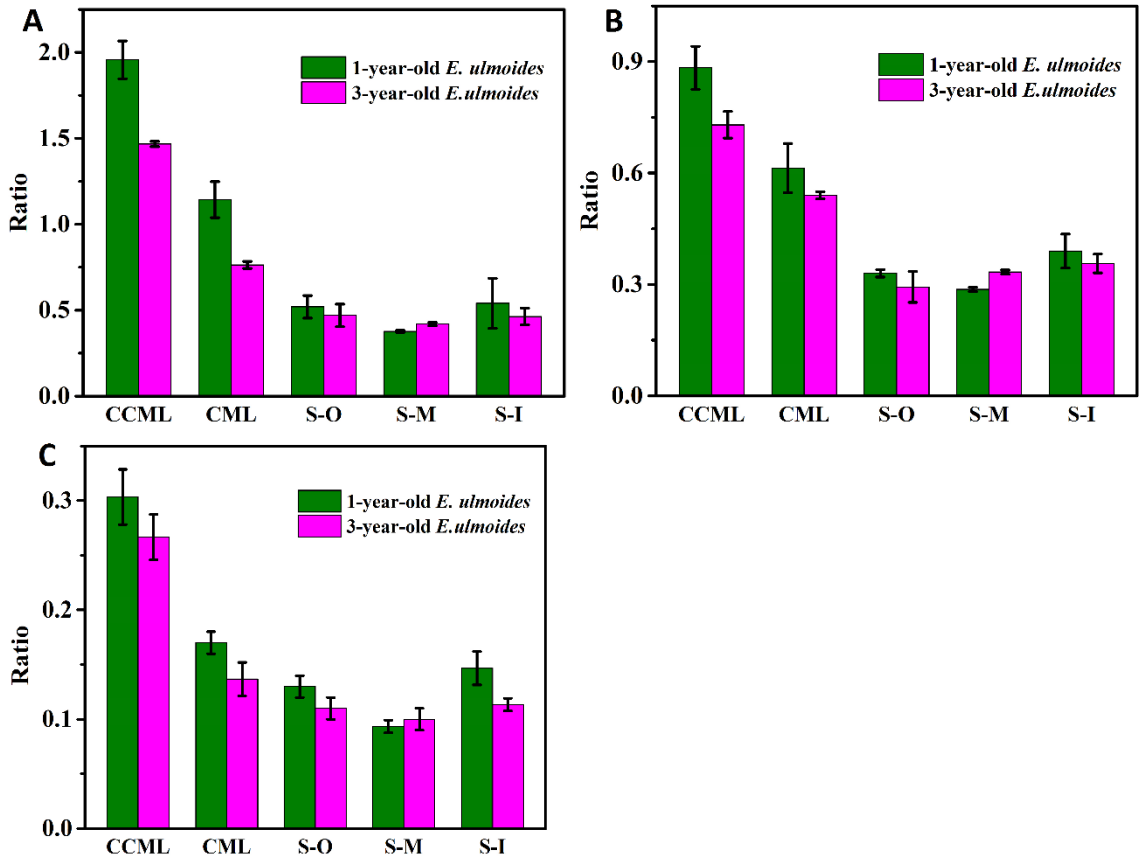

Fig. 6. The details of concentration ratio of lignin to carbohydrates (A: I_{1598}/I_{2889}, B: I_{1333}/I_{2889}, and C: I_{1274}/I_{2889}). CCML: cell corner middle lamella; CML: compound middle lamella; S-O: outer-layer; S-M: middle-layer; and S-I: inner-layer

Previously, the ratio of lignin-to-carbohydrate has been identified as a dominant factor influencing the recalcitrance to sugar release (Davison *et al.* 2006). Yoshida *et al.* (2014) indicated that decreasing the lignin-to-carbohydrate ratio from 0.39 to 0.1 effectively improves the saccharification efficiency. Similarly, Studer *et al.* (2011) found a strong negative correlation between sugar release and the ratio of lignin-to-carbohydrates. When the ratio was 0.38, the conversion of carbohydrates into fermentable sugar was 30%. However, a lower ratio (0.2) indicated that the negative influence of lignin was less apparent and that the sugar release was 60% higher. The increase in digestibility from combined pretreatment and enzymatic hydrolysis with a decreased concentration ratio of lignin-to-carbohydrates was mainly related to the more labile β-O-4 bonds in S-lignin during the pretreatment (Kishimoto *et al.* 2010). Since it has been confirmed that lower ratio of lignin-to-carbohydrate could be more helpful to increase the sugar release in fermentation process, 1-year-old *E. ulmoides* with lower ratio of lignin-to-carbohydrate than 3-year-old *E. ulmoides* would be preferable raw materials for biofuels.

The confocal Raman microscopy has been widely used to monitor lignocellulosic biomass cell wall dynamic changes during pretreatment for enhanced enzymatic digestibility (Zhang *et al*. 2014; Ji *et al*. 2015; Li *et al*. 2015). Also, the topochemical correlation between lignin and carbohydrates in different species, the same species of different age, or the location and tissues can be investigated by confocal Raman microscopy. Thus, it would be an efficient way to help to optimize raw materials and technology for biofuels production.

Although traditional microanalytical techniques, including ultraviolet microspectrophotometry, polarized light microscope, transmission electron microscope combined with immunocytochemistry, and fluorescence microscopy, have been comprehensively employed to investigate the distribution of lignin and carbohydrates (Vigneshwaran *et al.* 2011; Donaldson and Knox 2012; Andersson *et al.* 2015a; Zeng *et al.* 2015), these measurements require chemical treatment or complicated embedding procedure that may inevitably cause changes in the cell structure and modify cell wall components. On the contrary, spectroscopic methods, such as infrared (IR) and Raman spectroscopies measurements can provide complementary information about the molecular vibrations and be performed on the samples without any preparatory steps. However, IR spectroscopy is sensitive to water interference in the sample, since IR absorption is pronounced for polar molecules. In combination with microscopy, Raman spectroscopy has the advantage that spectra can be acquired on acquired on aqueous, thicker (not opaque) samples with a higher spatial resolution (Hänninen *et al.* 2011). Therefore, the confocal Raman microscopy is a preferable measurement to investigate the topochemical correlation between carbohydrates and lignin.

CONCLUSIONS

1. Overlaying the Raman image of carbohydrates and lignin revealed the colocalization of carbohydrates and lignin within the middle lamella and the secondary wall of fibers. However, examining the concentration distribution of the carbohydrates and lignin separately indicated that the regions with high carbohydrates had low lignin concentration or *vice versa*.
2. The Raman band intensity ratios of $I_{1274/2889}$ and $I_{1274/2889}$ revealed that a higher G- and S-lignin-to-carbohydrate ratio was present in the S-M region of *E. ulmoides*, while in the middle lamella, S-O, and S-I the ratio displayed the opposite trend.
3. Owing to the higher lateral resolution, easy handling, and simultaneous detection of multi-components, Confocal Raman microscopy has been shown to be an effective tool to evaluate the biomass chemical compositions and their ratio at the cellular and sub-cellular level, which will help to optimize raw materials and monitor the compositional changes of the matrix during biomass pretreatment and enzymatic hydrolysis. More importantly, when combined with wet chemistry analytical approaches, the whole view of biorefinery would be drawn at multiscale.

ACKNOWLEDGEMENTS

This study was funded by the National Natural Science Foundation of China (NO. 31500497) and the National "Twelfth Five Year" Science and Technology Support (NO. 2012BAD54G0103).

REFERENCES CITED

Andersson, S., Guna, N., Koch, G., Andersone, I., Feldmane, A. M., Biziks, V., Irbe, I., and Grinins, J. (2015a). "Scanning UV microspectrophotometry as a tool to study the changes of lignin in hydrothermally modified wood," *Holzforschung* 70(3), 215-221. DOI: 10.1515/hf-2015-0027

Andersson, S., Wang, Y., Pönni, R., Hänninen, T., Mononen, M., Ren, H., Serimaa, R., and Saranpää, P. (2015b). "Cellulose structure and lignin distribution in normal and compression wood of the Maidenhair tree (*Ginkgo biloba* L.): Properties of the *Ginkgo biloba* cell wall," *Journal of Integrative Plant Biology* 57(4), 388-395. DOI: 10.1111/jipb.12349

Agarwal, U. P. (2006). "Raman imaging to investigate ultrastructure and composition of plant cell walls: Distribution of lignin and cellulose in black spruce wood (*Picea mariana*)," *Planta* 224(5), 1141-1153. DOI: 10.1007/s00425-006-0295-z

Agarwal, U. P., and Atalla, R. H. (2010). "Vibrational spectroscopy," in: *Lignin and Lignans: Advances in Chemistry*, J. A. Schmidt (ed.), C. Heitner, D. R. Dimmel, Boca Raton, pp. 103-136.

Agarwal, U. P, McSweeny, J. D., and Ralph, S. A. (2011). "FT-Raman investigation of milled wood lignins: Softwood, hardwood, and chemically modified black spruce lignins," *Journal of Wood Chemistry and Technology* 31(4), 324-344. DOI: 10.1080/02773813.2011.562338

Atalla, R. H., and Agarwal, U. P. (1986). "*In situ* Raman microprobe studies of plant cell walls: Macromolecular organization and compositional variability in the secondary wall of *Picea mariana* (Mill.) B.S.P," *Planta* 169(3), 325-332. DOI: 10.1007/B00392127

Davison, B. H., Drescher, S. R., Tuskan, G. A., Davis, M. F., and Nghiem, N. P. (2006). "Variation of S/G ratio and lignin content in a *Populus* family influences the release of xylose by dilute acid hydrolysis," *Applied Biochemistry and Biotechnology* 129-132(1), 427-35. DOI: 10.1385/ABAB:130:1:427

Donaldson, L. A. (1993). "Mechanical constraints on lignin deposition during lignification," *Wood Science and Technology* 28(2), 111-118. DOI: 10.1007/BF00192690

Donaldson, L. A., and Knox, J. P. (2012). "Localization of cell wall polysaccharides in normal and compression wood of radiata pine: Relationships with lignification and microfibril orientation," *American Society of Plant Biologists* 158(2), 642-653. DOI: 10.1104/pp.111.184036

Hänninen, T., Kontturi, E., and Vuorinen, T. (2011). "Distribution of lignin and its coniferyl alcohol and coniferyl aldehyde groups in *Picea abies* and *Pinus sylvestris* as observed by Raman imaging," *Phytochemistry* 2(14-15), 1889-1895. DOI: 10.1016/j.phytochem.2011.05.005

Hu, W. R., Fan, L., Xie, L. X., and Wang, L. L. (2016). "Dynamic changes of lignin deposition during cotton fiber development stage," *Agricultural Sciences of Xinjiang* 53(3), 467-472. DOI: 10.6048/j.issn.1001-4330.2016.03.011

Ji, Z., Zhang, X., Ling, Z., Zhou, X., Ramaswamy, S., and Xu, F. (2015). "Visualization of *Miscanthus* × *giganteus* cell wall deconstruction subjected to dilute acid pretreatment for enhanced enzymatic digestibility," *Biotechnology for Biofuels* 8(1),1-14. DOI: 10.1186/s13068-015-0282-3

Jungnikl, K., Koch, G., and Burgert, I. (2008). "A comprehensive analysis of the relation of cellulose microfibril orientation and lignin content in the S2 layer of different tissue types of spruce wood (*Picea abies* (L.) Karst.)," *Holzforschung* 62(62), 475-480. DOI: 10.1515/HF.2008.079

Kanbayashi, T., and Miyafuji, H. (2015). "Raman microscopic analysis of wood after treatment with the ionic liquid, 1-ethyl-3-methylimidazolium chloride," *Holzforschung* 69(3), 273-279. DOI: 10.1515/hf-2014-0060

Kim, J. S., Sandquist, D., Sundberg, B., and Daniel, G. (2012). "Spatial and temporal variability of xylan distribution in differentiating secondary xylem of hybrid aspen," *Planta* 235(6), 1315-1330. DOI: 10.1007/s00425-011-1576-8

Kishimoto, T., Chiba, W., Saito, K., Fukushima, K., Uraki, Y., and Ubukata, M. (2010). "Influence of syringyl to guaiacyl ratio on the structure of natural and synthetic lignins," *Journal of Agricultural and Food Chemistry* 58(2), 895-901. DOI: 10.1021/jf9035172

Larsen, K. L., and Barsberg, S. (2010). "Theoretical and Raman spectroscopic studies of phenolic lignin model monomers," *Journal of Physical Chemistry B* 114(23), 8009-8021. DOI: 10.1021/jp1028239

Li, X., Ximenes, E., Kim, Y., Slininger, M., Meilan, R., and Ladisch, M. (2010). "Lignin monomer composition affects Arabidopsis cell-wall degradability after liquid hot water pretreatment," *Biotechnology for Biofuels* 3(46), 1-7. DOI: 10.1186/1754-6834-3-27

Li, H. Y., Sun, S. N., Wang, C. Z., and Sun, R. C. (2015). "Structural and dynamic changes of lignin in Eucalyptus cell walls during successive alkaline ethanol treatments," *Industrial Crops and Products* 74, 200-208. DOI: 10.1016/j.indcrop.2015.04.048

Li, Y. X., and Lei, Y. F. (2016). "Chemical components and their variations along tree stem of young branches of *Ramulus mori*, *Eucommia ulmoides* and *Tamarix ramosissma*," *Journal of Northwest and University* 44(5), 127-132. DOI: 10.13207/j.cnki.jnwafu.2016.05.017

Marjamaa, K., Lehtonen, M., Lundell, T., Toikka, M., Saranpää, P., and Fagerstedt, K. V. (2003). "Developmental lignification and seasonal variation in beta-glucosidase and peroxidase activities in xylem of Scots pine, Norway spruce and silver birch," *Tree Physiology* 23(14), 977-986. DOI: 10.1093/treephys/23.14.977

Moniz, P., Lino, J., Duarte, L. C., Roseiro, L. B., Boeriu, C. G., Pereira, H., and Cravalheiro, F. (2015). "Fractionation of hemicelluloses and lignin from rice straw by combining autohydrolysis and optimized mild organosolv delignification," *BioResources* 10(2), 2626-2641. DOI: 10.15376/biores.10.2.2626-2641

Prats, M. B., Hauser, M. T., Heredia, A., and Gierlinger, N. (2016). "Waterproofing in Arabidopsis: Following phenolics and lipids *in situ* by confocal Raman microscopy," *Frontiers in Chemistry* 4, 306. DOI: 10.3389/fchem.2016.00010

Richter, S., Müssig, G., and Gierlinger, N. (2011). "Functional plant cell wall design revealed by the Raman imaging approach," *Planta* 233(4), 763-772. DOI: 10.1007/s00425-010-1338-z

Raut, M. P., Couto, N., Pham, T. K., Evans, C., Noirel, J., and Wright, P. C. (2016). "Quantitative proteomic analysis of the influence of lignin on biofuel production by *Clostridium acetobutylicum*," *Biotechnology for Biofuels* 9(1), 1-16. DOI: 10.1186/s13068-016-0523-0

Ruel, K. (2004). "Immunolabelling of lignin sub-structures: A strategy for wood fibre wall

topochemical analyses," in: *Wood Fibre Cell Walls: Methods to Study their Formation, Structure, and Properties*, U. Schmitt, P. Ander, J. R. Barnett, A. M. C. Emons, G. Jeronimidis, P. Saranpa¨a¨, S. Tschegg (eds.), Uppsala University, Uppsala, Sweden, pp. 131-140.

Sluiter, A., Hames, B., Ruiz, R., Scarlata, C., Sluiter, J., Templeton, D., and Crocker, D. (2008). *Determination of Structural Carbohydrates and Lignin in Biomass* (NREL/TP-510-42618), National Renewable Energy Laboratory, Golden, CO.

Song, Y., Zhang, J., Zhang, X., and Tan, T. (2015). "The correlation between cellulose allomorphs (I and II) and conversion after removal of hemicellulose and lignin of lignocellulose," *Bioresource Technology* 193, 164-170. DOI: 10.1016/j.biortech.2015.06.084

Studer, M. H., DeMartini, J. D., Davis, M. F., Sykes, R. W., Davison, B., Keller, M., Tuskan, G. A., and Wyman, C. E. (2011). "Lignin content in natural *Populus* variants affects sugar release," *Proceedings of the National Academy of Sciences of the United States of America* 108(15), 6300-6305. DOI: 10.1073/pnas.1009252108

Sun, L., Varanasi, P., Yang, F., Loqué, D., Simmons, B. A., and Singh, S. (2012). "Rapid determination of syringyl: Guaiacyl ratios using FT-Raman spectroscopy," *Biotechnology and Bioengineering* 109(3), 647-656. DOI: 10.1002/bit.24348

Vigneshwaran, N., Ammayappan, L., and Huang, Q. (2011). "Effect of gum arabic on distribution behavior of nanocellulose fillers in starch film," *Applied Nanoscience* 1(3), 137-142. DOI: 10.1007/s13204-011-0020-5

Xu, J. K., Sun, Y. C., and Sun, R. C. (2015). "Synergistic effects of ionic liquid plus alkaline pretreatments on eucalyptus: Lignin structure and cellulose hydrolysis," *Process Biochemistry* 50(6), 955-965. DOI: 10.1016/j.procbio.2015.03.014

Yin, Y. F., Jiang, X. M., and Chao, Q. U. (2004). "Dynamic changes of lignin deposition in secondary xylem cell wall during secondary xylem differentiation in *Populus tomentosa* Carr.," *Journal of Chinese Electron Microscopy Society* 23(6), 663-669. DOI: 10.3969/j.issn.1000-6281.2004.06.016

Yoshida, M., Liu, Y., Uchida, S., Kawarada, K., Ukagami, Y., Ichinose, H., Kaneko, S., and Fukuda, K. (2014). "Effects of cellulose crystallinity, hemicellulose, and lignin on the enzymatic hydrolysis to monosaccharides," *Bioscience Biotechnology and Biochemistry* 72(3), 805-810. DOI: 10.1271/bbb.70689

Yuan, T. Q., Sun, S. N., Xu, F., and Sun, R. C. (2011). "Characterization of lignin structures and lignin-carbohydrate complex (LCC) linkages by quantitative 13C and 2D HSQC NMR spectroscopy," *Journal of Agricultural and Food Chemistry* 59(19), 10604-10614. DOI: 10.1021/jf2031549

Yu, Q., Zhuang, X., Yuan, Z., Kong, X., Qi, W., Wang, W., Wang, Q., and Tan, X. (2015). "Influence of lignin level on release of hemicellulose-derived sugars in liquid hot water," *International Journal of Biological Macromolecules* 82, 967-72. DOI: 10.1016/j.ijbiomac.2015.10.045

Zeng, Y. N., Zhao, S., Yang, S., and Ding, S. Y. (2014). "Lignin plays a negative role in the biochemical process for producing lignocellulosic biofuels," *Current Opinion in Biotechnology* 27(6), 38-45. DOI: 10.1016/j.copbio.2013.09.008

Zeng, Y. N., Zhao, S., Wei, H., Tucker, M. P., Himmel, M. E., Mosier, N. S., Meilan, R., and Ding, S. Y. (2015). "*In situ* micro-spectroscopic investigation of lignin in poplar cell walls pretreated by maleic acid," *Biotechnology for Biofuels* 8(1), 1-12. DOI: 10.1186/s13068-015-0312-1

Zhang, X., Ma, J., Ji, Z., Yang, G. H., Zhou, X., and Xu, F. (2014). "Using confocal Raman microscopy to real-time monitor poplar cell wall swelling and dissolution during ionic liquid pretreatment," *Microscopy Research and Technique* 77(8), 609-618. DOI: 10.1002/jemt.22379

Article submitted: September 16, 2016; Peer review completed: November 25, 2016; Revised version received and accepted: December 12, 2016; Published: December 15, 2016.
DOI: 10.15376/biores.12.1.1064-1076